IOP Publishing Journal of Physics: Condensed Matter
J. Phys.: Condens. Matter **31** (2019) 505703 (8pp) https://doi.org/10.1088/1361-648X/ab4094

Structural properties of protective diamond-like-carbon thin films grown on multilayer graphene

Jian Liu[1,2], **Henrique Vázquez Muíños**[1], **Kai Nordlund**[1] **and Flyura Djurabekova**[1]

[1] Helsinki Institute of Physics and Department of Physics, University of Helsinki, POB 43, 00014, Helsinki, Finland
[2] Department of Nuclear Science and Technology, Nanjing University of Aeronautics and Astronautics, Nanjing 210016, People's Republic of China

E-mail: flyura.djurabekova@helsinki.fi

Received 5 June 2019, revised 6 August 2019
Accepted for publication 2 September 2019
Published 20 September 2019

Abstract

In spite of the versatility of electronic properties of graphene, its fragility and low resistance to damage and external deformations reduce the practical value of this material for many applications. Coating of graphene with a thin layer of hard amorphous carbon is considered as a viable solution to protect the 2D material against accidental scratches and other external damaging impacts. In this study, we investigate the relationship between the deposition condition and quality of diamond-like-carbon (DLC) on top of multilayer graphene by means of molecular dynamics simulations. Deposition of carbon atoms with 70 eV incident energy at 100 K resulted in the highest content of sp^3-bonded C atoms. An increase of the number of dangling bonds at the interface between the top graphene layer and the DLC film indicates that decrease of the incident energy reduces the adhesion quality of DLC thin film on graphene. Analysis of radial distribution function indicates that sp^3 hybridized carbon atoms tend to grow near already existing sp^3-atoms. This explains why the quality of the DLC structures grown on graphene have generally a lower content of sp^3 C atoms compared to those grown directly on diamond. Ring analysis further shows that a DLC structure grown on the sp^2-rich structures like graphene contains a higher fraction of disordered ring structures.

Keywords: diamond-like-carbon, multilayer graphene, molecular dynamics, carbon atoms deposition

(Some figures may appear in colour only in the online journal)

1. Introduction

With the rapid development of nanoscience and nanotechnology, carbon nanomaterials, such as fullerenes [1], carbon nanotubes [2] and graphene [3], have gained much attention. Many scientific efforts are dedicated to study the properties and investigate potential applications of these carbon nanomaterials. Amongst these, graphene is the most promising stable 2D material. Its unique properties such as mechanical resistance [4], electrical [5] and thermal [6] conductivity, etc, compared to conventional macro-materials make graphene a promising material in various applications such as gas sensing [7], water purification [8], and touch screens [9] in the future. However, the attractive properties of graphene can alter severely due to mechanical wearing, scratching [10], or parasitic irradiation in space applications [11, 12]. The damage of graphene in daily used graphene-based appliances and equipments, will surely shorten the serving time of the latter. Thus, it is of great importance to find a compatible durable coating to protect graphene and enhance its resistant ability against external damage.

Diamond-like-carbon (DLC) is reported to be in many ways an ideal protective material for nanostructures and is

able to enhance mechanical strength of nanomaterials [13–15]. DLC exhibits many desirable properties, such as ultra-high hardness and elastic moduli [16], low friction coefficient [17], transparency in the IR wavelength band [18] and chemical inertness [19]. Moreover, it is highly compatible with graphene structure. DLC coatings are widely used in many applications, e.g. as an antireflection layer for IR optic devices [20], a protection layer for magnetic storage components [21] and an anticorrosion layer for biocompatible materials [22]. It will be utilized extensively even more in various fields like electronics, aviation, aerospace, etc [23–25]. In addition, some research has been carried out to analyze the protective properties of DLC films coating nanostructure both experimentally [15, 26–31] and by simulations [32–34]. In particular, Ren *et al* [35] analyzed the effect of experimental conditions such as the combination of incident energy and ambient temperature on the quality of growing DLC film directly on diamond and on nanotubes placed on a diamond substrate, showing that a stable DLC can grow above a nanotube structure. The above-mentioned research shows that it is feasible to grow a DLC protective layer on top of carbon nanostructures. However, it is not entirely clear what defines the quality of the grown DLC films, in order to predict their protective properties. Unfortunately there are only a few reports about the quality of DLC deposited on top of graphene in different conditions. DLC, which is a variety of amorphous carbon, shows diverse properties with a different ratio of sp^2 and sp^3 hybridization [36]. It was seen that the higher sp^3 fraction the DLC has, the harder and denser it becomes [37]. Therefore, in the current paper we aim to find out how the deposition condition during the growth of thin films can define the quality of DLC above graphene, in order to enable the growth of high quality DLC protective layers.

Atomistic simulation methods are powerful tools to study mechanisms of atomic migration and collision, and eventually, the formation of the bonds within the materials [38, 39]. In this paper, we utilized classical molecular dynamics (MD) to simulate and study the process of carbon ion beam deposition with different incident energies at 100 K on the top of multilayer graphene. Recently, Caro *et al* [40] develops a new type of potentials, which are based on Machine-learning technique. While being quite advanced and able to predict the formation of sp^3 bonds versus sp^2 during the deposition at room temperature, this type of potentials is very slow and is not suited for analysis of radiation damage. In our work, we chose the recipe of reducing the deposition temperature and optimizing the deposition incident energy to enable formation of DLC of three different sp^3 content. Then, we analyzed the atomic structure, density and sp^3 fraction of grown DLC films in different conditions in order to reveal what inherent mechanisms lead to failure of growth of stable and dense DLC structures.

2. Simulation and analysis methods

Simulations of DLC deposition process shown in this paper were carried out with classical MD code PARCAS [41, 42]. In order to describe the interaction between carbon atoms,

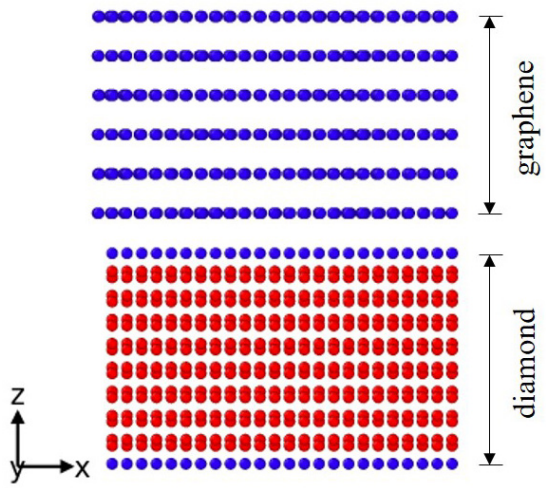

Figure 1. Schematic diagram of diamond and multilayer graphene model. Red atoms represent sp^3 hybridization while blue atoms stand for sp^2 hybridization.

the empirical analytical bond-order Brenner–Beardmore potential [43–45] was applied. We used the extended low-end ($R = 1.95$ Å) and high-end ($S = 2.25$ Å) cutoff parameters, following Jäger and Albe's work [46], to improve the description of formation of sp^3-hybridization of carbon atoms. The extended cutoffs allowed depositing DLC with higher sp^3 fraction, which compares better to experimentally grown DLC films [35]. None of the classical potentials are able to predict fully correctly the formation of sp^3 bonded atoms [47, 48], however, the selected potential with the extended cutoff has been shown to describe well [35] the fact that the maximal sp^3 content in DLC is obtained at about 70 eV [49]. In the previous study [35], it was also found that simulations done at 100 K give sp^3 to sp^2 content fractions that are well in line with DLC experiments. Hence most of the work in this article is also carried out at 100 K. All the visualized simulation cells in this paper were obtained with the help of open visualization tool OVITO [50].

Figure 1 shows the schematic diagram of the initial multilayer graphene placed on top of the diamond substrate. For the sake of convenience, all sp^3-hybridized C atoms are colored red in this and the following figures, while sp^2-hybridized C atoms are colored blue. This structure was built up as follows. The diamond substrate with the $\langle 111 \rangle$ surface normal and the size of $30 \times 30 \times 20$ Å included 3456 atoms. Six layers of graphene, 2304 atoms, were placed above the diamond substrate with the layer spacing of 3.35 Å (the interlayer distance in graphite), and the distance between diamond surface and bottom graphene was also 3.35 Å. To minimize the energy of multilayer graphene system, all the six layers of graphene were stacked in the A-B Bernal order. Third, periodic boundary condition was set in lateral (x and y) directions, leaving the z-direction an open surface to deposit DLC.

We used the Berendsen [51] thermostat to control the temperature at the lateral borders within the 5 Å region and the two bottom layers of diamond atoms were fixed in order to dissipate heat and prevent the entire system from moving downwards during the continuous carbon ion beam

irradiation. At last, incident carbon atoms were set 5 Å above the top layer of graphene with the velocity directed perpendicular to the graphene layers in the direction of the surface. The incident energies for the deposition process was varied between 50, 70, and 100 eV, in different sets of the subsequent deposition simulations. Before each carbon atom impact, a random cell shift in the *xy* plane was performed to ensure that carbon atoms would hit the whole graphene layer uniformly. Each ion impact was simulated for the total time of 10 ps to allow the generated heat to dissipate naturally at the boundaries of the simulation cell. As carbon atoms were arriving on graphene, the DLC film was gradually growing up and the initial incident position of depositing carbon atoms was also shifted up to ensure that there is always 5 Å distance to the highest *z*-coordinate of an atom in the cell to avoid extreme repulsive forces caused due to inappropriately short distances between newly appeared incident atom and already existed DLC. The ambient temperature was set as 100 K during the DLC film deposition. For each energy, around 8000 carbon impacts were carried out to obtain the desired volume of DLC for further analysis.

To evaluate the quality of the grown DLC film, we analyzed the sp^3 fraction, mass density, radial distribution function (RDF), and primitive rings in all the grown structures. We set the first cutoff length as 1.9 Å, as an average value between the first and the second peaks in the total RDF, respectively; see figure 4. All the atoms with the coordination number less than or equal to three within the selected cutoff were considered as three-bonded carbon atoms, or as the sp^2 hybridized ones (the same as in [52]), while four-bonded atoms are counted as having sp^3 hybridization. Apart from the total RDF for all atoms, we also computed the RDF for only the sp^2 and the sp^3 hybridized atoms to deconvolute the total RDF and analyze the short range order of both types of atoms in the grown DLC films. To inspect the total disorder degree, we also performed the primitive rings analysis [53]. In addition, the dangling bonds of carbon atoms located in the interface between graphene surface and bottom of the DLC were also analyzed to evaluate adhesion quality of the DLC film.

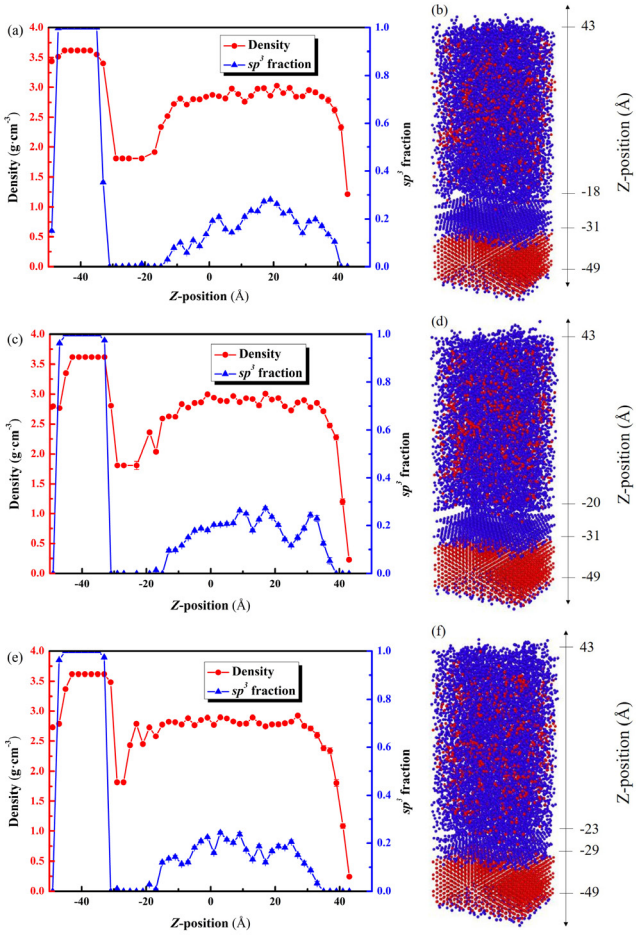

Figure 2. sp^3 fraction (right-hand *y*-axis) and mass density (left-hand *y*-axis) of the simulation cells as a function of *z*-coordinate with the incident energies of (a) 50 eV, (c) 70 eV, and (f) 100 eV. The corresponding post-deposition simulation cells are shown in (b), (d), and (f), respectively. Red circles indicate the atoms with sp^3-hybridized bonds and blue are the atoms with sp^2 ones. The error bars show the standard deviation in the analysis of all the atoms in the corresponding structure.

3. Results and discussion

3.1. sp^3 fraction and mass density

Figure 2 shows the distribution of the sp^3 fraction and mass density of the low-energy-ion deposited DLC film with the different incident energies along the *z*-axis (perpendicular to the surface) and corresponding simulation cells at 100 K and incident energies of 50, 70, and 100 eV, respectively. The four ticks to the right of the simulation cells are used to guide the eye to the location of the bottom and the top of the simulation cells, as well as of both interfaces (diamond-graphene and graphene-DLC). These four positions corresponds to four turning points in the relevant graphs; see figures 2(a), (c) and (e). In all these subfigures, the diamond and graphene regions are well visible, since diamond has a maximum density of 3.6 g cm^{-3} and consists of pure sp^3 carbon atoms while graphene has minimum density of 1.8 g cm^{-3} and is made of pure sp^2 carbon atoms. As the *z*-coordinate increases, the average density increases fluctuating around 2.7 g cm^{-3}. At the same time, some increase in the sp^3 fraction is also observed. This behavior of the mass density and sp^3 fraction indicate the presence of the grown DLC film. We note here that the number of the sp^3-hybridized atoms is slightly higher in the middle of the cell, further away from the interface and the open surface, where excess of the free volume can impede formation of the sp^3-bonds, as expected from the conventional subplantation model of DLC formation [54, 55]. The stress exerted on sp^2 carbon atoms by deposition of energetic carbon atoms and the continuously growing DLC film breaks the π C–C bond, converting it into a σ C–C bond. This process results in formation of four σ covalent bonds corresponding to sp^3 hybridization instead of three σ and one π bonds corresponding to the sp^2 hybridization. On the other hand, due to the abundance of the sp^2-hybridized carbon atoms in graphene, the first layer of the growing film (right above graphene layers) consists mainly of the same sp^2 carbon atoms, constituting the loose amorphous carbon structure at the bottom of the DLC film.

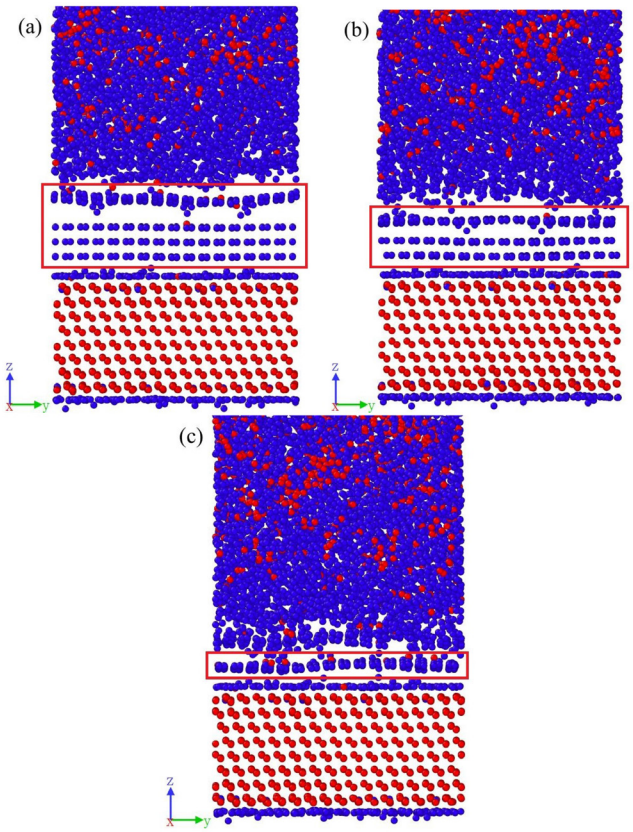

Figure 3. Partial enlargement of lower part of deposited structure in figure 2 from side view under (a) 50, (b) 70, and (c) 100 eV, respectively. Remaining graphene layers are in red rectangles.

While analyzing the sp^3 fractions in the DLC grown structures with different incident energies, we see that most sp^3 fractions form in DLC films grown with 70 eV incident energies than other two energies. This indicates that there exists an optimal incident energy to form highest sp^3 fraction. On the other hand, from figure 3, we can observe clearly that graphene layers at diamond side can still be intact since the incident carbon atoms are of low kinetic energy and blocked by upper graphene layers. Meanwhile, with the increase of incident energy, fewer layers of graphene remain intact. For 50 eV, there are still four layers of graphene existing while three layers survived after 70 eV bombardment. In the case of 100 eV, only one graphene layer is clearly visible and separate from above DLC.

Reduction of the number of graphene layers means that graphene is partially consumed by the DLC film during the growing process and some of the sp^2 carbon atoms from the original graphene layers transformed in the sp^3 hybridized atoms. Hence, the average sp^3 fraction obtained in the cell grown at 100 K with the 70 eV incident carbon ions is higher than that of 50 eV. Although higher deposition energy increases the conversion of the activated graphene sp^2 atoms to become part of the DLC film, it also means that the sp^2-to-sp^3 conversion is promoted due to sufficient local stress generated by more energetic ions capable of penetrating deeper into the cell, compared to those of 50 eV energy. This effect makes a notable difference only at low temperature like 100 K, since low temperature helps it stabilize the local concentration of the stress. Since sp^2 covalent C–C bonds are energetically more favorable [56], any temperature increase (also due to energetic ion impacts) in the disordered structure of amorphous carbon may reduce the local stress, causing spontaneous transition of forming sp^3 C–C bonds into sp^2 C–C bonds, reducing overall the sp^3 fraction.

Table 1. Mass density (g cm^{-3}) and sp^3 content (%) of DLC films deposited at different incident energies. The values are averaged over the whole DLC layer; in the center the sp^3 content is higher.

Energy (eV)	Mass density (g cm^{-3})	sp^3 content (%)
50	2.728	14.9
70	2.766	15.9
100	2.704	13.8

The mass density of the DLC films grown under different conditions along with the corresponding sp^3 content are listed in table 1. We note that the simulation process of the film growth is time-consuming, which is why we report here the results of analysis of a single structure for each energy, aiming mainly at qualitative comparison of different deposition conditions. The density and sp^3 fraction combination in our work is close to the simulation results that Wang *et al* [57] calculated via tight-binding molecular dynamics. In this table, we see that the sp^3 fraction shows much stronger dependence on the incident energy than the average mass density of the grown DLC.

To investigate this effect further, we plot the radial distribution functions for two grown DLC structures with the highest and lowest content of sp^3 atoms to identify the difference in the short range order of all the carbon atoms within these structures. Figure 4 shows the radial distribution function grown with 70 and 100 eV, as well as deconvolution of the peak into the sp^2 and sp^3 components. We show all bonds within the high-end cutoff parameter 2.25 Å of the Brenner potential, which includes only the first nearest neighbors. We see that the expected value of the bond length in the entire structure that was grown at 100 K is around 1.49 $\pm$ 0.07 Å and is independent of incident energy. Hereafter the error bars indicate the standard deviation in the value of the bond length for all the atoms in the corresponding structure.

When we analyze separately the expected values of the sp^2- and sp^3-bond lengths, we found them to be the same in both structures shown in figure 4 and amounted to 1.46 $\pm$ 0.04 Å and 1.6 $\pm$ 0.09 Å, respectively. We see that the average bond length in the grown DLC structures for the sp^2-bonded atoms is very close to that in ideal graphene (1.42 Å), while the sp^3-bonds are slightly stretched. Also there is some variation in the mean values of the sp^3-bond lengths, compared to diamond (bond length 1.54 Å), because of the relatively small number of atoms with such bonds; the amount of these atoms clearly affects the average bond length in the entire structure.

Overall, in both cases we observe a much higher peak of the sp^2-bonds compared to sp^3 ones as seen in figure 4, even for the best structures with the highest density and highest sp^3-content. As was shown in [35], sp^3 carbon atoms tend to

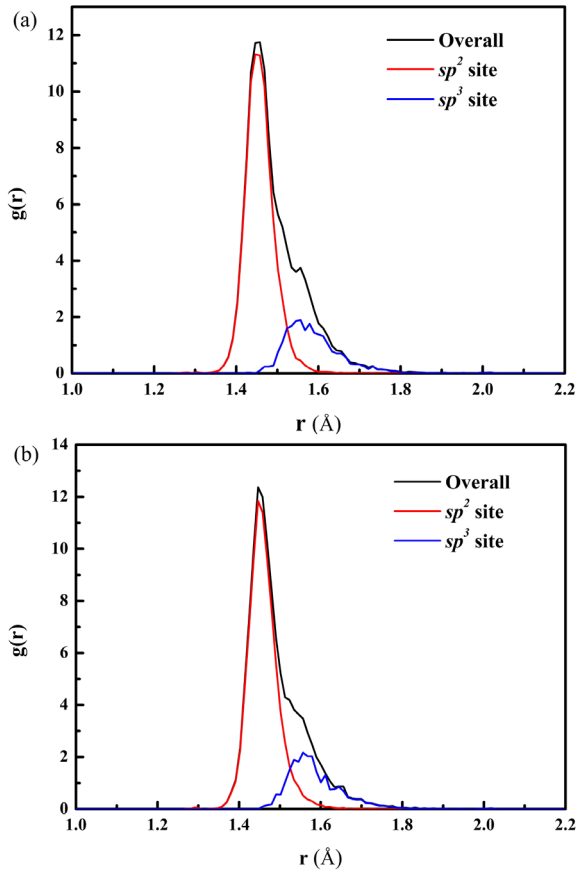

Figure 4. Radial distribution function $g(r)$ for DLC deposited at 100 K under incident energies of (a) 70 and (b) 100 eV, respectively. The contributions of sp^2 and sp^3 coordination are presented separately in red and blue.

grow near the atoms which already are sp^3-bonded as in diamond. Since we deposited the DLC film on top of graphene layers, the deposited atoms were landing next to the atoms with the sp^2-bonding, forming the same sp^2-bonds in more preferable manner. In other words, we observe the lack of formation of the sp^3-bonded carbon atoms during the initial stage of film deposition, which is consistent with the observations in [35].

It is obvious that the mass densities increase with sp^3 content in the grown film, in agreement with experiment [55]. Because the bond length of the sp^2-hybridized atoms is shorter than sp^3 bonds, intutively it seems that it can contain more sp^2 carbon atoms than sp^3 atoms within unit volume. However, the density of graphite, which is made up of pure sp^2 carbon atoms, is much lower than diamond. In graphite, this inconsistency is explained by the large interlayer distance, while the interlayer distance in amorphous carbon is ill-defined. This is why we further analyze the average atomic volume, instead of simply examining bond length, in the DLC structures with the highest and the lowest sp^3 fraction. For this purpose we employ the Voronoi tessellation analysis available in OVITO software. According to this analysis, the average atomic volumes in multilayer graphene and diamond are 9.233 ± 0.345 Å^3 and 5.678 ± 0.001 Å^3, respectively.

Table 2. Average atomic volume with the standard deviation calculated for the carbon atoms in the DLC films deposited at different temperatures and incident energies.

	Average atomic volume (Å^3)	
Energy (eV)	sp^2 atoms	sp^3 atoms
50	7.53 ± 1.59	6.08 ± 0.65
70	7.44 ± 1.12	6.12 ± 0.66
100	7.58 ± 1.31	6.15 ± 0.61

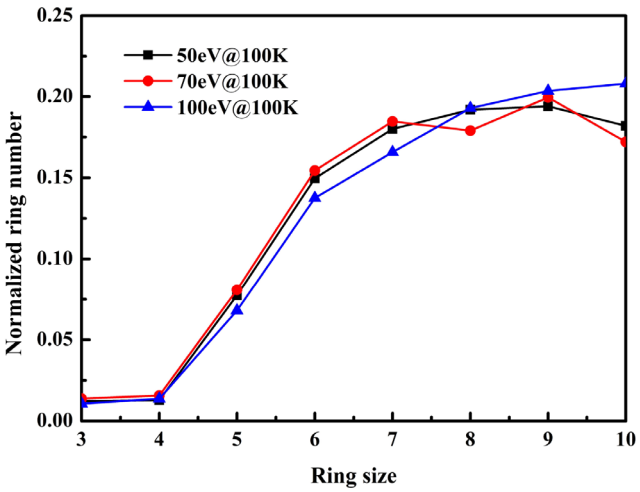

Figure 5. Normalized ring number as a function of ring size at 100 K under 50, 70, and 100 eV, respectively.

In table 2, we list the average atomic volume separately for sp^2 and sp^3 atoms in DLC films deposited at different incident energies at 100 K. We see that the average atomic volume is larger in the cells with the lowest content of sp^3 bonding, which explains the lower mass density. It is surprising that the atomic volume for the sp^3-bonded atoms is very similar in all structures although it is slightly larger than in pure diamond. This indicates that the formed sp^3 atoms are stable and the bond stretching is mainly explained by the large amount of the sp^2-bonded atoms, which occupy much larger volume per atom. The slightly smaller atomic volume for the sp^2-bonded atoms are explained by densification during the impact.

3.2. Ring analysis

Different atomic volumes occupied by the sp^2-bonded atoms indicates that there can be structural differences in the grown films. To investigate the nature of this differences, we performed the analysis of the primitive rings [53] for quantitative investigation of the degree of long range disorder in the deposited DLC films. We chose the same structures as analyzed in figure 2, namely the films grown at 100 K with all three incident energies. For this analysis we used the method described in [53], excluding the top 20 Å of the DLC structure.

In figure 5, we see that the three DLC structures grown at 100 K have similar distributions of the primitive rings. We see mainly the seven- to ten-member rings, although the number of the six-member rings is only slightly smaller than the larger rings. The five-member rings are quite prominent in these

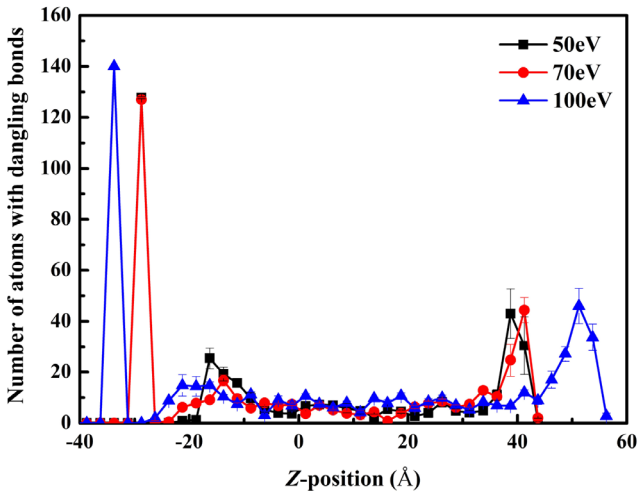

Figure 6. Number of atoms with dangling bonds as a function of z-position under different incident energies at 100 K. Each data point is averaged on the last frame of the last 10 incidenting and with error bars representing standard deviation.

structures as well. We see that the amount of the primitive rings with the large number members starts decreasing above eight-member rings in the films with larger quantity of the sp^3 atoms, while the film grown with the 100 eV incident energy exhibits the presence of the primitive rings with the higher number of ten-member rings, which indicates the reduction of structural quality of the film. In figure 5, we observe much higher fraction of nine- and ten-member rings than in [35]. This could be attributed to the relatively low sp^3 fraction in table 1 compared to [35], and the six-element ring represents the structure more close to diamond and is the prefect primitive ring structure. Even so, DLC generated under 100 eV shows more disordered structure than that under 50 and 70 eV due to the relatively low fraction of six-element rings and high fraction of ten-element rings, meaning that 100 eV produced poorer quality of DLC comparing to other two energies when considering previous data and analysis. DLC deposited under 70 eV is only less disordered in a tiny degree than that under 50 eV comparing the six- and other-element rings. Hence, considering the sp^3 fraction, mass density, and disorder degree, we can draw the conclusion that 70 eV incident energy will lead to better quality of DLC deposited by carbon atoms continuously implanting.

3.3. Dangling bonds

The quality of DLC film is defined not only by the high sp^3 fraction and mass density, but also by the strength of adhesion of the film to the graphene top layer. Loose adhesion of the film to the substrate may result in sliding of the film along the graphene surface under external force. Since the C–C covalent bonds are strong and stable, the atoms with less neighbors than three at least will weaken the adhesion ability of the film in general. In figure 6, we plot the number of atoms with dangling bonds (<3 neighbors) as a function of the z-coordinate. We also observe clear peaks at the positions corresponding to the interfaces between diamond and graphene, graphene and DLC, and at the open surface of DLC film. Unsaturated dangling bonds increase the energy of the interface, reducing the barrier needed to detach the DLC film from the graphene surface.

Since we are interested in the interface between graphene and DLC, in this study we focus on the second peak from the left in figure 6. Different symbols in the same plot show the results obtained at 100 K with different incident energies. In figure 6, there are slightly less atoms with dangling bonds created by ions with 100 eV than with 70 eV and the largest number of the dangling bonds is observed for the lowest incident energy. This clearly indicates that the high incident energy decreases the number of dangling bonds due to more intensive displacement cascades and activated atoms, which helps energetic atoms at the interface to form bonds with others. The analysis of the content of dangling bonds in the graphene-DLC interface shows a clear competition between the thermal and radiation-induced processes. In this study, the ambient temperature (100 K) is quite low. Therefore, the thermal velocities are very small and the atoms do not have opportunity to saturate the dangling bonds without additional energy introduced by an impacting ion.

Based on this analysis, we conclude that the quality of film adhesion to multilayer graphene increases with increasing incident energy that counterbalanced by the poorer quality of the grown film structure at high energy. This is why it is important to optimize the film growth condition by carefully selecting the energy of carbon ions during the deposition of the film. Since the peaks for the dangling bonds at this interface created by 70 and 100 eV are almost the same, we conclude that the ions with 70 eV transfer the optimal amount of energy to the lattice atoms to maximize the effect of bond saturation and protect more beneath graphene layers. At lower energy, the transferred energy may not be sufficient and at higher energy induces too strong movement of atoms that the bonds remain dangling and also graphene layers are consumed (see the remaining intact graphene layers).

4. Conclusions

In this study, we analyzed the quality of the DLC films deposited on multilayer graphene as a protective layer with different energy of incident carbon ions. We showed that in spite of sp^2-bonding of carbon atoms in graphene, which impedes the formation of sp^3-hybridization, a DLC film can grow above graphene by careful selection of optimal deposition condition. We saw that sp^3 hybridization tends to appear in the middle part of DLC along z-direction due to the pressure induced transformation from sp^2 to sp^3 hybridization. Deposition at 70 eV resulted in the highest fraction of sp^3-bonded atoms and the highest mass density. They dropped with both increasing and decreasing incident energies. Higher incident energy leaves fewer intact graphene layers after deposition. For 100 eV case, five layers of graphene were destroyed and only one layer remains obviously visible. In the films, the sp^2-bond length was very close on average to that of graphene, while the sp^3-bond length was slightly longer than that in diamond.

Clearly the atomic volume occupied by the sp^2-bonded atoms was much larger than that of sp^3-bonded atoms, but yet, much smaller than in multilayer graphene. By analyzing the primitive rings in the grown structures, we also concluded that the DLC grows above graphene is mainly disordered structure with a small amount of stable five- and six-member rings. At the same time, the quality of the film adhesion improved with increase of incident energy at 100 K. The best adhesion was achieved with the energy of 100 eV. After comprehensive consideration of various situations, we concluded that 70 eV incident energy can provide best quality of DLC film, while it can also retain the good adhesion ability with graphene layers.

Acknowledgments

We acknowledge the support provided by China Scholarship Council (CSC) during a visit of Jian Liu to University of Helsinki. We also acknowledge grants of computer capacity from the IT Centre for Science in Finland, CSC and the Finnish Grid and Cloud Infrastructure (persistent identifier urn:nbn:fi:research-infras-2016072533). This work is also supported by the Postgraduate Research & Practice Innovation Program of Jiangsu Province (Grant No. KYLX15_0306) and the Fundamental Research Funds for the Central Universities (Grant Nos. NJ20150021 and NJ20170012).

ORCID iDs

Jian Liu https://orcid.org/0000-0001-9961-4544
Henrique Vázquez Muíños https://orcid.org/0000-0003-1697-9797

References

[1] Murayama H, Tomonoh S, Alford J M and Karpuk M E 2005 Fullerene production in tons and more: from science to industry *Fuller. Nanotub. Car. N.* **12** 1–9
[2] Baughman R H, Zakhidov A A and De Heer W A 2002 Carbon nanotubes—the route toward applications *Science* **297** 787–92
[3] Huang H, Tang X, Chen F, Liu J, Li H and Chen D 2016 Graphene damage effects on radiation-resistance and configuration of copper–graphene nanocomposite under irradiation: a molecular dynamics study *Sci. Rep.* **6** 39391
[4] Mohan V B, Souri H, Jayaraman K and Bhattacharyya D 2018 Mechanical properties of thin films of graphene materials: a study on their structural quality and functionalities *Curr. Appl. Phys.* **18** 879–85
[5] Sun H, Fu C, Gao Y, Guo P, Wang C, Yang W, Wang Q, Zhang C, Wang J and Xu J 2018 Electrical property of macroscopic graphene composite fibers prepared by chemical vapor deposition *Nanotechnology* **29** 305601
[6] Qin G, Qin Z, Wang H and Hu M 2018 On the diversity in the thermal transport properties of graphene: a first-principles-benchmark study testing different exchange-correlation functionals *Comput. Mater. Sci.* **151** 153–9
[7] de Souza F A, Amorim R G, Prasongkit J, Scopel W L, Scheicher R H and Rocha A R 2018 Topological line defects in graphene for applications in gas sensing *Carbon* **129** 803–8
[8] Dervin S, Dionysiou D D and Pillai S C 2016 2d nanostructures for water purification: graphene and beyond *Nanoscale* **8** 15115–31
[9] Khan U, Kim T-H, Ryu H, Seung W and Kim S-W 2017 Graphene tribotronics for electronic skin and touch screen applications *Adv. Mater.* **29** 1603544
[10] Lee M-S *et al* 2013 High-performance, transparent, and stretchable electrodes using graphene–metal nanowire hybrid structures *Nano Lett.* **13** 2814–21
[11] Liu X, Pu J, Wang L and Xue Q 2013 Novel dlc/ionic liquid/graphene nanocomposite coatings towards high-vacuum related space applications *J. Mater. Chem.* A **1** 3797–809
[12] Siochi E J 2014 Graphene in the sky and beyond *Nat. Nanotechnol.* **9** 745
[13] Robertson J 1992 Properties of diamond-like carbon *Surf. Coat. Tech.* **50** 185–203
[14] Voevodin A, Donley M and Zabinski J 1997 Pulsed laser deposition of diamond-like carbon wear protective coatings: a review *Surf. Coat. Tech.* **92** 42–9
[15] Wei C, Yang J-F and Tai F-C 2010 The stress reduction effect by interlayer deposition or film thickness for diamond like carbon on rough surface *Diam. Relat. Mater.* **19** 518–24
[16] Won Y J and Ki H 2014 Effect of film gradient profile on adhesion strength, residual stress and effective hardness of functionally graded diamond-like carbon films *Appl. Surf. Sci.* **311** 775–9
[17] Ankit K, Varade A, Reddy N, Dhan S, Chellamalai M, Krishna P and Balashanmugam N 2017 Synthesis of high hardness, low COF diamond-like carbon using RF-PECVD at room temperature and evaluating its structure using electron microscopy *Diam. Relat. Mater.* **80** 108–12
[18] Klyui N, Liptuga A, Lozinskii V, Lukyanov A, Oksanich A and Terban V 2012 Application of diamond-like carbon films to increase transmission of semi-insulating gaas crystals in the ir spectral range *Tech. Phys. Lett.* **38** 609–12
[19] Bewilogua K and Hofmann D 2014 History of diamond-like carbon films—from first experiments to worldwide applications *Surf. Coat. Tech.* **242** 214–25
[20] Ankit K, Varade A, Reddy N, Dhan S, Chellamalai M, Balashanmugam N and Krishna P 2017 Synthesis of high hardness IR optical coating using diamond-like carbon by PECVD at room temperature *Diam. Relat. Mater.* **78** 39–43
[21] Goglia P R, Berkowitz J, Hoehn J, Xidis A and Stover L 2001 Diamond-like carbon applications in high density hard disc recording heads *Diam. Relat. Mater.* **10** 271–7
[22] Grill A 2003 Diamond-like carbon coatings as biocompatible materials—an overview *Diam. Relat. Mater.* **12** 166–70
[23] Bai L, Zhang G, Lu Z, Wu Z, Wang Y, Wang L and Yan P 2011 Tribological mechanism of hydrogenated amorphous carbon film against pairs: a physical description *J. Appl. Phys.* **110** 033521
[24] Donnet C and Erdemir A 2004 Historical developments and new trends in tribological and solid lubricant coatings *Surf. Coat. Tech.* **180** 76–84
[25] Shi W, Wei X, Zhang W, Wang Z, Dong C and Li S 2017 Developments and applications of diamond-like carbon *Appl. Mech. Mater.* **864** 14–24
[26] Schittenhelm H, Geohegan D B, Jellison G, Puretzky A A, Lance M J and Britt P F 2002 Synthesis and characterization of single-wall carbon nanotube–amorphous diamond thin-film composites *Appl. Phys. Lett.* **81** 2097–9
[27] Kinoshita H, Ippei I, Sakai H and Ohmae N 2007 Synthesis and mechanical properties of carbon nanotube/diamond-like carbon composite films *Diam. Relat. Mater.* **16** 1940–4
[28] Lettington A H 1998 Applications of diamond-like carbon thin films *Carbon* **36** 555–60
[29] Varshney D, Weiner B R and Morell G 2010 Growth and field emission study of a monolithic carbon nanotube/diamond composite *Carbon* **48** 3353–8

[30] Sakudo N, Ikenaga N, Yasui H and Awazu K 2008 Amorphous carbon coating mixed with nano-diamonds *Thin Solid Films* **516** 4483–6
[31] Zhang J, Yu Y and Huang D 2010 Good electrical and mechanical properties induced by the multilayer graphene oxide sheets incorporated to amorphous carbon films *Solid State Sci.* **12** 1183–7
[32] Baimova J, Rysaeva L K and Rudskoy A 2018 Deformation behavior of diamond-like phases: molecular dynamics simulation *Diam. Relat. Mater.* **81** 154–60
[33] Wang Y, Xu J, Ootani Y, Bai S, Higuchi Y, Ozawa N, Adachi K, Martin J M and Kubo M 2017 Tight-binding quantum chemical molecular dynamics study on the friction and wear processes of diamond-like carbon coatings: effect of tensile stress *ACS Appl. Mater. Inter.* **9** 34396–404
[34] Wang Y, Xu J, Zhang J, Chen Q, Ootani Y, Higuchi Y, Ozawa N, Martin J M, Adachi K and Kubo M 2018 Tribochemical reactions and graphitization of diamond-like carbon against alumina give volcano-type temperature dependence of friction coefficients: a tight-binding quantum chemical molecular dynamics simulation *Carbon* **133** 350–7
[35] Ren W, Iyer A, Koskinen J, Kaskela A, Kauppinen E I, Avchaciov K and Nordlund K 2015 Conditions for forming composite carbon nanotube-diamond like carbon material that retain the good properties of both materials *J. Appl. Phys.* **118** 194306
[36] McKenzie D 1996 Tetrahedral bonding in amorphous carbon *Rep. Prog. Phys.* **59** 1611
[37] Robertson J 2002 Diamond-like amorphous carbon *Mater. Sci. Eng.* R **37** 129–281
[38] Huang H, Tang X, Chen F, Liu J and Chen D 2017 Role of graphene layers on the radiation resistance of copper–graphene nanocomposite: Inhibiting the expansion of thermal spike *J. Nucl. Mater.* **493** 322–9
[39] Li X, Ke P, Zheng H and Wang A 2013 Structural properties and growth evolution of diamond-like carbon films with different incident energies: A molecular dynamics study *Appl. Surf. Sci.* **273** 670–5
[40] Caro M A, Deringer V L, Koskinen J, Laurila T and Csányi G 2018 Growth mechanism and origin of high sp^3 content in tetrahedral amorphous carbon *Phys. Rev. Lett.* **120** 166101
[41] Nordlund K, Ghaly M, Averback R, Caturla M, de La Rubia T D and Tarus J 1998 Defect production in collision cascades in elemental semiconductors and fcc metals *Phys. Rev.* B **57** 7556
[42] Ghaly M, Nordlund K and Averback R 1999 Molecular dynamics investigations of surface damage produced by kiloelectronvolt self-bombardment of solids *Phil. Mag.* A **79** 795–820
[43] Brenner D W 1990 Empirical potential for hydrocarbons for use in simulating the chemical vapor deposition of diamond films *Phys. Rev.* B **42** 9458
[44] Brenner D W 1992 Erratum: Empirical potential for hydrocarbons for use in simulating the chemical vapor deposition of diamond films *Phys. Rev.* B **46** 1948
[45] Beardmore K and Smith R 1996 Empirical potentials for C-Si-H systems with application to C_{60} interactions with Si crystal surfaces *Phil. Mag.* A **74** 1439–66
[46] Jäger H and Albe K 2000 Molecular-dynamics simulations of steady-state growth of ion-deposited tetrahedral amorphous carbon films *J. Appl. Phys.* **88** 1129–35
[47] Marks N 2002 Modelling diamond-like carbon with the environment-dependent interaction potential *J. Phys.: Condens. Matter* **14** 2901
[48] de Tomas C, Suarez-Martinez I and Marks N A 2016 Graphitization of amorphous carbons: a comparative study of interatomic potentials *Carbon* **109** 681–93
[49] Hakovirta M, Salo J, Lappalainen R and Anttila A 1995 Correlation of carbon ion energy with sp^2sp^3 ratio in amorphous diamond films produced with a mass-separated ion beam *Phys. Lett.* A **205** 287–9
[50] Stukowski A 2009 Visualization and analysis of atomistic simulation data with OVITO–the open visualization tool *Model. Simul. Mater. Sci.* **18** 015012
[51] Berendsen H J, Postma J V, van Gunsteren W F, DiNola A and Haak J 1984 Molecular dynamics with coupling to an external bath *J. Chem. Phys.* **81** 3684–90
[52] Kupka K *et al* 2018 Graphitization of amorphous carbon by swift heavy ion impacts: molecular dynamics simulation *Diam. Relat. Mater.* **83** 134–40
[53] Yuan X and Cormack A 2002 Efficient algorithm for primitive ring statistics in topological networks *Comput. Mater. Sci.* **24** 343–60
[54] Lifshitz Y, Kasi S, Rabalais J and Eckstein W 1990 Subplantation model for film growth from hyperthermal species *Phys. Rev.* B **41** 10468
[55] Fallon P, Veerasamy V, Davis C, Robertson J, Amaratunga G, Milne W and Koskinen J 1993 Properties of filtered-ion-beam-deposited diamondlike carbon as a function of ion energy *Phys. Rev.* B **48** 4777
[56] Liu J, Tang X, Li Y, Dai Z, Chen F, Huang H, Li H, Liu H and Chen D 2017 Effects of irradiation-induced structure evolution on the adhesion force and instantaneous modulus of multi-walled carbon nanotube arrays *Mater. Chem. Phys.* **196** 160–9
[57] Wang C Z, Ho K M and Chan C T 1993 Tight-binding molecular-dynamics study of amorphous carbon *Phys. Rev. Lett.* **70** 611